Thy1$^+$IL-7$^+$ lymphatic endothelial cells in iBALT provide a survival niche for memory T-helper cells in allergic airway inflammation

Kenta Shinoda[a], Kiyoshi Hirahara[a,b], Tomohisa Iinuma[b,c], Tomomi Ichikawa[a], Akane S. Suzuki[d], Kaoru Sugaya[a], Damon J. Tumes[a], Heizaburo Yamamoto[c], Takahiro Hara[e], Shizue Tani-ichi[e], Koichi Ikuta[e], Yoshitaka Okamoto[c], and Toshinori Nakayama[a,f,1]

[a]Department of Immunology, Graduate School of Medicine, Chiba University, Chiba 260-8670, Japan; [b]Department of Advanced Allergology of the Airway, Graduate School of Medicine, Chiba University, Chiba 260-8670, Japan; [c]Department of Otorhinolaryngology, Graduate School of Medicine, Chiba University, Chiba 260-8670, Japan; [d]Department of Medical Immunology, Graduate School of Medicine, Chiba University, Chiba 260-8670, Japan; [e]Laboratory of Biological Protection, Department of Biological Responses, Institute for Virus Research, Kyoto University, Kyoto 606-8507, Japan; and [f]AMED-CREST, AMED, Chiba 260-8670, Japan

Edited by Jason G. Cyster, University of California, San Francisco, CA, and approved April 8, 2016 (received for review June 26, 2015)

Memory CD4$^+$ T helper (Th) cells are central to long-term protection against pathogens, but they can also be pathogenic and drive chronic inflammatory disorders. How these pathogenic memory Th cells are maintained, particularly at sites of local inflammation, remains unclear. We found that ectopic lymphoid-like structures called inducible bronchus-associated lymphoid tissue (iBALT) are formed during chronic allergic inflammation in the lung, and that memory-type pathogenic Th2 (Tpath2) cells capable of driving allergic inflammation are maintained within the iBALT structures. The maintenance of memory Th2 cells within iBALT is supported by Thy1$^+$IL-7–producing lymphatic endothelial cells (LECs). The Thy1$^+$IL-7–producing LECs express IL-33 and T-cell–attracting chemokines CCL21 and CCL19. Moreover, ectopic lymphoid structures consisting of memory CD4$^+$ T cells and IL-7$^+$IL-33$^+$ LECs were found in nasal polyps of patients with eosinophilic chronic rhinosinusitis. Thus, Thy1$^+$IL-7–producing LECs control chronic allergic airway inflammation by providing a survival niche for memory-type Tpath2 cells.

lymphatic endothelial cell | pathogenic Th2 cell | IL-7 | iBALT | chronic rhinosinusitis

Immunological memory is a key feature of adaptive immunity, and memory CD4$^+$ T cells are crucial for this system to function. In the absence of memory CD4$^+$ T cells, B-cell responses, including the generation of high-affinity memory B cells and long-lived plasma cells, are markedly impaired (1, 2). Moreover, CD4$^+$ T cells are required for the maintenance of memory CD8$^+$ T cells (3). In addition to their protective functions, memory CD4$^+$ T cells also play a central role in the pathogenesis of chronic inflammatory disorders, including asthma and atopic dermatitis (4, 5). IL-5–producing memory Th2 cell subsets are critical for the pathology of allergic inflammation, and function as "memory-type pathogenic Th2 cells" (6) (Tpath2 cells). Given the importance of memory CD4$^+$Th cells, little is known about how memory CD4$^+$Th cells are maintained in the body, especially at local inflammatory sites where they persist and induce chronic inflammation.

Bronchus-associated lymphoid tissue (BALT) develops as a normal mucosal lymphoid tissue observed in the lung in certain mammalian species, including rabbits and rats, but not humans or mice (7). In humans and mice, BALT is induced in the lung in response to inflammation caused by various infectious organisms, and is called inducible BALT (iBALT) (8). iBALT consists of separate B-cell and T-cell areas, with the presence of resident dendritic cells (DCs), follicular DCs (FDCs), high endothelial venules (HEVs), and lymphatics (8, 9). Some similarities between the processes of iBALT generation and the preprogrammed development of conventional lymph nodes have been reported (10). For instance, the chemokine CXCL13 (the ligand for CXCR5) and the chemokines CCL19 and CCL21 (ligands for CCR7) are involved in formation of iBALT as well as lymphoid neogenesis (11). Moreover, mice deficient in the chemokine receptor CCR7 appear to spontaneously develop BALT together with excessive formation of secondary lymphoid organs without being exposed to immunological stimulation (12). In humans, iBALT formation has been identified in patients with chronic inflammatory diseases such as rheumatoid arthritis, tuberculosis, and chronic obstructive pulmonary diseases (13–15). Despite increasing evidence of the correlation between iBALT formation and the severity of chronic inflammatory diseases in the lung, the pathophysiological roles of iBALT remain unknown.

Chronic rhinosinusitis (CRS) involves long-term inflammation of the nasal and paranasal sinus mucosa (16). CRS is one of the most common comorbidities among patients with asthma, and the comorbidities share similar inflammatory processes and histopathology (17). CRS has been recently divided into two subgroups: with and without nasal polyps (18). The majority of cases of CRS with nasal polyps show Th2-type inflammation with prominent accumulation of eosinophils in the nasal polyps and are thus called eosinophilic CRS (ECRS) (19). Histological

Significance

A substantial proportion of people have intractable chronic allergic diseases for which no curative treatment exists. A clear understanding of how these allergic diseases develop and persist is lacking. Here, unique ectopic lymphoid-like structures called inducible bronchus-associated lymphoid tissue were found to be formed during chronic airway inflammation, and were critical in persistent inflammation. In addition, we identified a Thy1$^+$IL-7$^+$IL-33$^+$ subset of lymphatic endothelial cells (LECs) that support the maintenance of memory-type pathogenic T helper 2 (Tpath2) cells. A similar population of IL-7$^+$IL-33$^+$ LECs was found in nasal polyps of patients with eosinophilic chronic rhinosinusitis. Thus, we revealed that Thy1$^+$IL-7–producing LECs control chronic allergic airway inflammation by supporting memory-type Tpath2 cells in human and mouse systems.

Author contributions: K. Shinoda, K.H., Y.O., and T.N. designed research; K. Shinoda, K.H., T. Iinuma, T. Ichikawa, A.S.S., K. Sugaya, and H.Y. performed research; T.H., S.T., and K.I. contributed new reagents/analytic tools; K. Shinoda, K.H., T. Iinuma, T. Ichikawa, A.S.S., H.Y., Y.O., and T.N. analyzed data; and K. Shinoda, K.H., D.J.T., and T.N. wrote the paper.

The authors declare no conflict of interest.

This article is a PNAS Direct Submission.

Freely available online through the PNAS open access option.

[1]To whom correspondence should be addressed. Email: tnakayama@faculty.chiba-u.jp.

This article contains supporting information online at www.pnas.org/lookup/suppl/doi:10.1073/pnas.1512600113/-/DCSupplemental.

analysis of nasal polyps of patients with ECRS revealed massive tissue eosinophilia as well as infiltrating lymphocytes (20).

Herein, we demonstrate that Tpath2 cells are efficiently maintained in iBALT in the lung in a chronic allergic airway inflammation model. We identified Thy1$^+$IL-7–producing lymphatic endothelial cells (LECs) in the iBALT structures that support the maintenance of memory Th2 cells. In humans, lymphatics with IL-7$^+$IL-33$^+$ LECs, together with accumulation of ectopic lymphoid tissues containing memory CD4$^+$ T cells, were found in nasal polyps of patients with ECRS. Thus, in humans and mice, specialized Thy1$^+$IL-7$^+$IL-33$^+$ LECs appear to maintain pathogenic memory CD4$^+$ T cells within iBALT. Our study provides new insight into the mechanism through which memory-type pathogenic Th cells are maintained at local inflammatory sites and defines therapeutic targets for the treatment of chronic airway inflammation.

Results

Antigen-Specific Effector Th2 Cell Transfer Followed by Intranasal Antigen Exposure Induced iBALT Formation. For effective defense by memory T cells, some memory CD4$^+$ T cells reside within tissues at the interface between the body and the environment (21). However, it is unclear how pathogenic memory CD4$^+$ T cells that drive chronic inflammatory disorders are maintained in regions of peripheral inflammation. To address this question, we investigated local accumulation of memory T cells within inflamed lungs in response to intranasal (i.n.) administration of antigens in mice that had received effector Th2 cells by adoptive transfer (Fig. S1*A*). The i.n. administration of antigen resulted in massive perivascular and peribronchiolar infiltrates in the lung 42 d after effector cell transfer (the memory phase), whereas i.p. administration did not induce this response (Fig. 1*A*). The i.n. antigen administration selectively increased KJ1$^+$ memory Th2 cells in the lung (Fig. 1*B* and Fig. S1*B*), and the accumulation of memory cells persisted for at least 3 mo after i.n. administration of antigens (Fig. S1*C*). Memory Th2 cells in the lung showed higher expression of CD69 and CD25 compared with those in the spleen (Fig. S1*D*), and produced Th2 cytokines such as IL-4, IL-5, and IL-13 upon restimulation in vitro (Fig. S1*E*). Importantly, these locally accumulated memory Th2 cells did not show evidence of increased DNA synthesis measured by incorporation of BrdU or proliferation measured by Ki67 staining (Fig. S1 *F* and *G*).

Histological analysis of lungs of mice that had been administered i.n. antigen revealed the formation of iBALT, containing donor-derived KJ1.26 (KJ1)$^+$CD4$^+$ T cells, MHC class II$^+$ cells, and B220$^+$ cells (Fig. 1*C*, *Upper*), together with CD11c$^+$ cells (Fig. 1*C*, *Left*, *Lower*). Vascular cell adhesion molecule 1 (VCAM1)-expressing stromal cells and CD21-expressing follicular DCs (Fig. 1*C*, *Middle* and *Right*, *Lower*) were detected in the iBALT. Some peripheral node addressin (PNAd)-expressing HEVs were also detected (Fig. S1*H*). We then analyzed the distribution of KJ1$^+$ Th2 cells in the iBALT and lung parenchyma, and found that KJ1$^+$ Th2 cells had preferentially accumulated within areas of iBALT ($P = 0.0056$, two-tailed Student's t test) compared with nonlymphoid areas (Fig. 1*D*). Antigen-specific naive CD4$^+$ T cells did not induce iBALT formation, indicating the requirement for primary antigen encounter by the effector Th2 cells in this experimental system (Fig. S1*I*). Consistent with this result, i.n. administration of ovalbumin (OVA)/LPS to mice that had received a lower number (1×10^6) of naive CD4$^+$ T cells (Fig. S2*A*) also resulted in increased numbers of memory Th cells compared with mice that received OVA/LPS i.p. (Fig. S2*B*) and induced iBALT (Fig. S2*C*). Thus, the administration of effector Th2 cells followed by local administration of specific antigen induced iBALT formation, in which memory Th2 cells preferentially localized.

Eosinophilic Airway Inflammation Is Efficiently Induced in Mice That Have Developed iBALT. Next, we investigated the pathophysiological role of memory Th2 cells maintained within iBALT. We

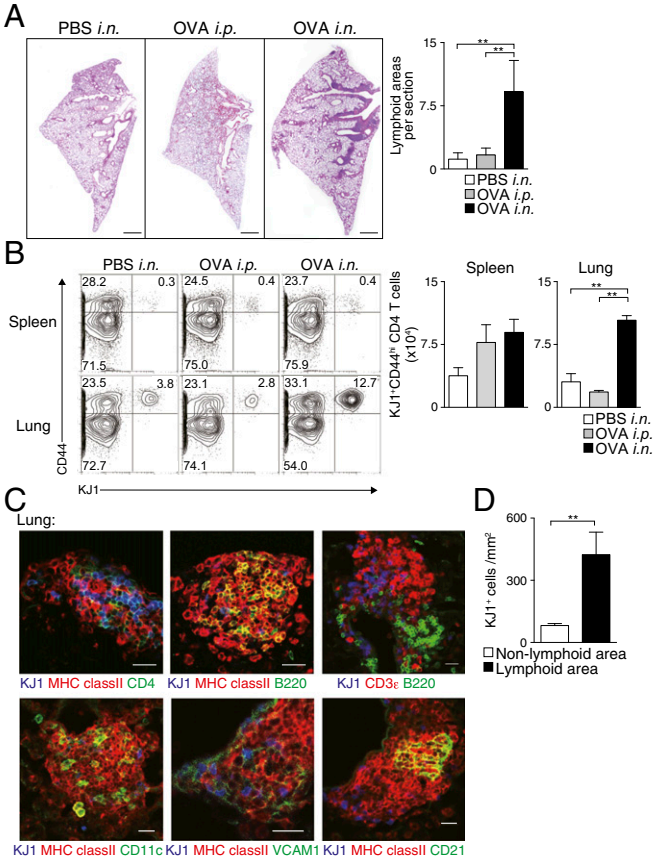

Fig. 1. Memory Th2 cells preferentially localized in iBALT. Effector Th2 cells from DO11.10 OVA-specific αβTCR Tg mice were transferred i.v. into BALB/c mice, which were subsequently challenged i.n. with OVA or PBS solution (control) or i.p. with OVA (control) at days 1 and 3, and the indicated assays were performed at day 42. (*A*) Representative cryosections of the lungs stained with H&E are depicted (*Left*), as is the absolute number of iBALT structures in the lungs (*Right*). (Scale bars, 1 mm.) Mean values with SD from at least three mice per group are shown. Two independent experiments were performed with similar results. (*B*) Representative staining profiles of CD44 and KJ1 expression on CD4$^+$ cells from the indicated organs (*Left*) and absolute cell numbers of KJ1$^+$CD44^{hi}CD4$^+$ T cells in the indicated organs (*Right*). Mean values with SD from five mice per group are shown. More than five independent experiments were performed with similar results. (*C*) Representative confocal micrograph of lung tissue stained with anti-KJ1 (blue), anti-MHC class II (red), and anti-CD4 (green) (*Upper Left*); anti-KJ1 (blue), anti-MHC class II (red), and anti-B220 (green) (*Upper Middle*); anti-KJ1 (blue), anti-CD3ε (red), and anti-B220 (green) (*Upper Right*); anti-KJ1 (blue), anti-MHC class II (red), and anti-CD11c (green) (*Lower Left*); anti-KJ1 (blue), anti-MHC class II (Red), and anti-VCAM1 (green) (*Lower Middle*); or anti-KJ1 (blue), anti-MHC class II (Red), and anti-CD21 (green) (*Lower Right*) are shown. (Scale bars, 40 μm.) More than three independent experiments were performed with similar results. (*D*) Morphometric analysis of KJ1$^+$ cells localized in lymphoid areas of the lungs is shown. Means and SD calculated from analysis of three slides per mouse from four mice. Two independent experiments were performed with similar results (**$P < 0.01$).

assessed OVA-induced airway inflammatory responses by using the mice in which iBALT formation had been induced as described earlier (Fig. S3*A*). After secondary antigen challenge, mice with iBALT showed significantly increased numbers of eosinophils and neutrophils ($P < 0.001$, Tukey's multiple comparisons test) in bronchioalveolar lavage (BAL) fluid compared with control groups in which antigen had been administered i.p. in the initial challenge and had thus not developed iBALT (Fig. 2*A*). Consistent with the cellular inflammatory profiles within BAL fluid, mucus hyperproduction and airway hyperresponsiveness were

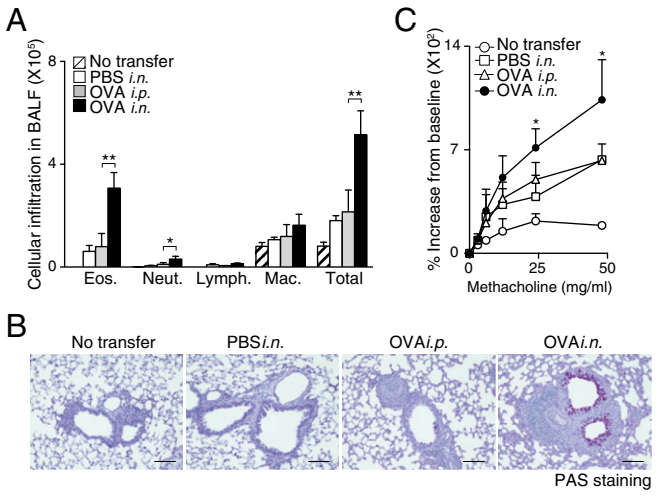

Fig. 2. iBALT formation accompanied by iBALT-residing memory Th2 cells caused severe airway inflammation. Mice with or without iBALT were treated with inhaled OVA on day 62 after Th2 cell transfer and i.n. challenge as described in Fig. 1. BAL fluid and airway hyperresponsiveness were assessed on day 63. (*A*) Absolute cell numbers of eosinophils (Eos.), neutrophils (Neut.), lymphocytes (Lymph.), and macrophages (Mac.) in the BAL fluid are shown. Mean values from five mice per group are shown with SD. (*B*) Microscopy of the lungs from mice as in *A*, fixed and stained with periodic acid-Schiff reagent. (Scale bars, 100 μm.) (*C*) Airway hyperresponsiveness was assessed by measuring methacholine-induced changes in lung resistance. Mean values for the percentage above baseline are shown for three to six mice in each group (**$P < 0.01$; and *$P < 0.05$). Two independent experiments were performed with similar results (*A*–*C*).

enhanced in the mice that had iBALT (Fig. 2 *B* and *C*). These results indicate that the memory Th2 cells in the mice with iBALT formation induced robust airway inflammation and airway hyperresponsiveness, both of which are characteristic pathologic processes of allergic asthma.

Memory Th2 Cells Are Maintained Within iBALT in an Antigen-Nonspecific Manner. To assess whether the accumulation and maintenance of memory Th2 cells in iBALT are antigen-specific events, two other lines of experiments were performed. T-cell receptor (TCR)-nontransgenic (Tg) polyclonal Th2 cells generated in vitro were labeled with 5-chloromethylfluorescein diacetate (CMFDA) and transferred into the mice in which iBALT was induced by OVA-specific effector Th2 cell transfer (Fig. 3*A*). IL-7Rα was expressed on transferred antigen-specific Th2 cells at similar levels at 1 wk and 4 wk after cell transfer (Fig. S3*B*). We first assessed cell numbers 1 wk after cell transfer to avoid fading of the fluorescence of transferred CMFDA-labeled cells. The number of polyclonal Th2 cells was higher ($P = 0.0023$, two-tailed Student's *t* test) in the lung of mice with iBALT compared with that in PBS solution-treated control mice (Fig. 3*B*). The polyclonal Th2 cells existed preferentially in iBALT regions (Fig. 3*C*). Next, we assessed whether OVA-specific TCR Tg Th2 cells were maintained efficiently in iBALT that was induced by LPS (Fig. 3*D*). We found that LPS-induced inflammation also resulted in the development of iBALT in the lungs (Fig. 3*E*). Importantly, the number of memory OVA-specific TCR Tg Th2 cells was higher ($P = 0.0011$, two-tailed Student's *t* test) in the lungs of mice that had generated iBALT in response to LPS compared with that in PBS solution-treated control mice (Fig. 3*F*). Again, the OVA-specific TCR Tg Th2 cells existed preferentially in the iBALT region (Fig. 3*G*). When unprimed polyclonal CD4 T cells (5×10^6) were transferred together with OVA-specific effector Th2 cells (5×10^6; Fig. S4*A*), more OVA-specific effector Th2 cells were present after 1 wk (10.6%; Fig. S4*B*) compared with unprimed polyclonal CD4 T cells (0.5%; Fig. S4*C*). However, we still detected significant increases in numbers of unprimed polyclonal CD4 T cells in the lung if LPS was administered i.n. (Fig. S4*C*).

In addition, we investigated the pathophysiological role of memory Th2 cells maintained within iBALT that were induced by LPS (Fig. 3*H*). After secondary i.n. antigen challenge with OVA, the mice with preformed iBALT that was induced by i.n. administration of LPS showed significantly increased numbers of infiltrated eosinophils ($P = 0.0256$, two-tailed Student's *t* test) and neutrophils ($P = 0.0014$, two-tailed Student's *t* test) in BAL fluid compared with the mice without preformed iBALT (PBS solution i.n. + Th2 cell transfer group; Fig. 3*I*). Moreover, enhanced airway hyperresponsiveness was observed in the mice with preformed iBALT compared with the control group (Fig. 3*J*). These results indicate that memory Th2 cells accumulated and were maintained in iBALT in an antigen-nonspecific manner and strongly contribute to the pathology of local pulmonary inflammation.

IL-7 Supports the Maintenance of iBALT-Residing Memory Th2 Cells. As IL-7 is known to contribute to the maintenance of $CD4^+$ T cells in vivo (22, 23), the role of IL-7 in the maintenance of iBALT-residing memory Th2 cells was assessed by using IL-7:GFP knock-in mice. Ly5.1 OT-II Tg effector Th2 cells were transferred into IL-7:GFP knock-in mice (*Il-7*$^{gfp/+}$) and the accumulation of transferred OVA-specific memory Th2 cells in the lung was assessed on day 42 as depicted in Fig. S1*A*. The majority of the IL-7–producing cells were localized within iBALT in the lung (Fig. 4*A*, *Left*). Intriguingly, more than 90% of $Ly5.1^+$ memory Th2 cells were colocalized with IL-7–producing cells within the iBALT (Fig. 4*A*, *Right*, and Fig. 4*B*). We next sought to gain more insight into possible mechanisms through which IL-7 contributes to the maintenance of iBALT-residing memory Th2 cells. The addition of IL-7 to memory Th2 cells prepared from the lungs of mice with iBALT in in vitro cultures showed that IL-7 decreased apoptosis and increased expression of antiapoptotic Bcl2 protein in memory Th2 cells ($P = 0.0008$ and $P = 0.0007$, respectively; Tukey's multiple comparisons test; Fig. 4*C*, *Left* and *Middle*). The rescue effect of IL-7 on apoptosis and up-regulation of Bcl2 in memory Th2 cells was also inhibited by the addition of IL-7Rα neutralizing antibody in the culture ($P = 0.0058$ and $P = 0.0007$, respectively, Tukey's multiple comparisons test; Fig. 4*C*, *Right*). Consistent with these results, the treatment of recipient mice with anti–IL-7Rα antibody in vivo resulted in a significant reduction in number of memory Th2 cells maintained in iBALT of the lung ($P = 0.0268$, two-tailed Student's *t* test; Fig. 4*D*). To further investigate the nonredundant role of IL-7 in the maintenance of memory Th2 cells in iBALT, we analyzed memory Th2 cells from *Il7r* conditional KO mice crossed with Cre-ERT Tg mice (*Il7r*cKO mice) followed by 2 wk treatment of tamoxifen in vivo (Fig. S4*D*). The administration of tamoxifen did not affect the formation of iBALT structures; however, the number of memory Th2 cells in iBALT was significantly decreased ($P = 0.0016$, two-tailed Student's *t* test; Fig. 4 *E* and *F*). These results indicate that the maintenance of memory Th2 cells in iBALT is dependent on IL-7. Moreover, after secondary i.n. OVA challenge, *Il7r*cKO Th2 cell transferred mice showed significantly impaired numbers of infiltrated eosinophils ($P < 0.001$, Tukey's multiple comparisons test) in BAL fluid (Fig. 4*G*) and attenuated airway hyperresponsiveness (Fig. 4*H*). These results indicate that ameliorated airway inflammation is a result of the decrease in memory Th2 cells as a consequence of deletion of *Il7Rα*.

Thy1$^+$ IL-7–Producing LECs Provide a Survival Niche for Memory Th2 Cells in iBALT. IL-7 is produced by stromal cells in lymphoid organs and by $VCAM1^+$ cells in the bone marrow (24). In the lung, it has been reported that LECs produce IL-7 and are distributed

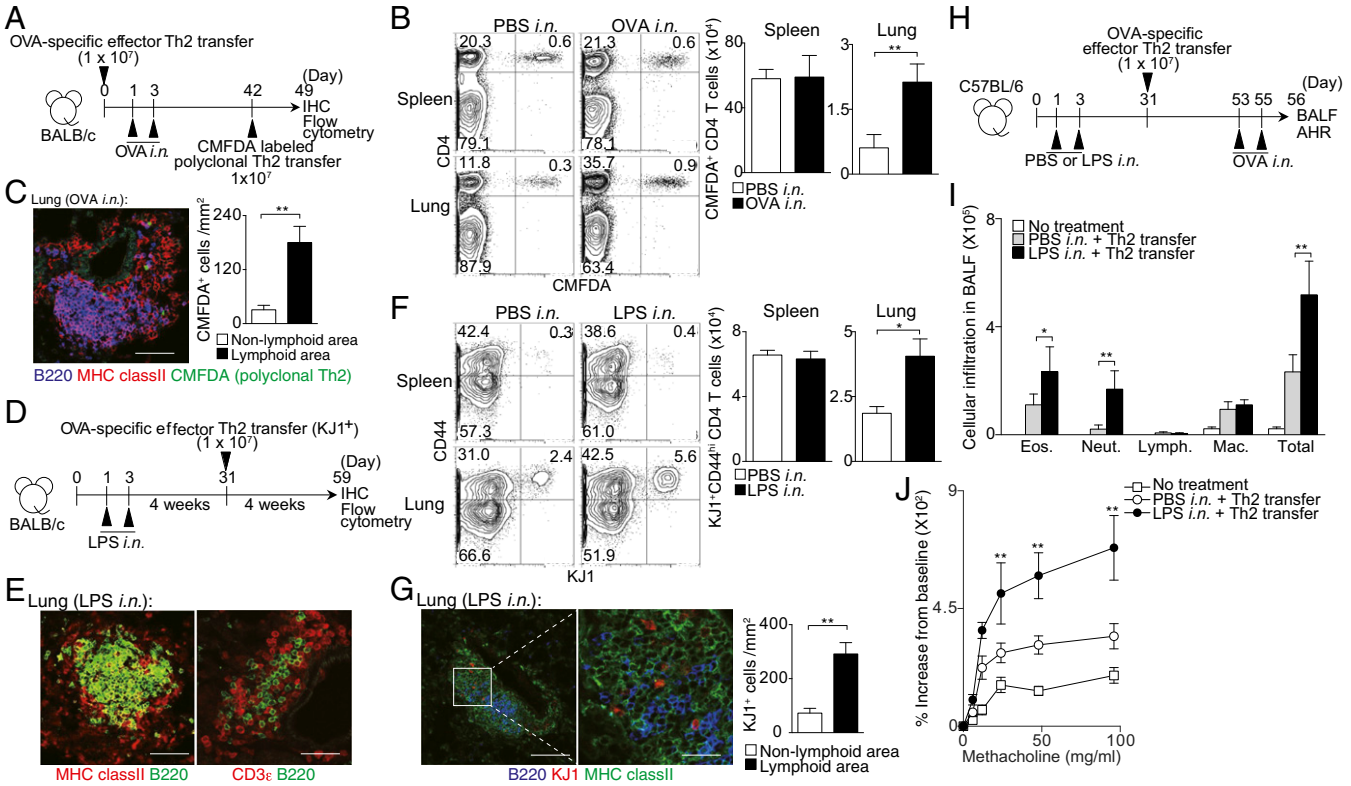

Fig. 3. Antigen-independent maintenance of memory Th2 cells in iBALT. (*A*) Splenic CD4$^+$ T cells from WT mice were cultured under Th2 conditions. These polyclonal Th2 cells were labeled with CMFDA and transferred into the mice 42 d after induction of iBALT as described in Fig. 1, and analyzed 1 wk later at day 49. (*B*) Representative staining profiles of CD4 and CMFDA in the indicated organs are shown. (*C*) Representative confocal micrographs of lung tissue from mice in *A* stained with anti-B220 (blue), anti-MHC class II (red), and CMFDA (green) (*Left*), and morphometric analysis of CMFDA$^+$ cells localized in lymphoid areas of the lungs (*Right*). (Scale bars, 100 μm.) (*D*) BALB/c mice were administered i.n. with LPS at days 1 and 3, and effector Th2 cells from DO11.10 OVA-specific αβTCR Tg mice were transferred i.v. at day 31, with analysis performed at day 59. (*E*) Representative confocal micrograph of lung tissue from mice in *D* stained with anti-MHC class II (red) and anti-B220 (green) (*Left*), and anti-CD3ε (red) and anti-B220 (green) (*Right*). (Scale bars, 40 μm.) (*F*) Representative staining profiles of CD44 and KJ1 expression on CD4$^+$ cells in the indicated organs. (*G*) Representative confocal micrograph of lung tissue from mice in *D* stained with anti-B220 (blue), anti-KJ1 (red), and anti-MHC class II (green) (*Left* and *Middle*), and morphometric analysis of KJ1$^+$ cells localized in lymphoid areas of the lungs (*Right*). (Scale bars: *Left*, 100 μm; *Middle*, 20 μm.) (*H*) C57BL/6 mice were administered i.n. with LPS on days 1 and 3, and effector Th2 cells from OT-II Tg mice were transferred i.v. at day 31. Mice were challenged i.n. with OVA on days 53 and 55, and BAL fluid and airway hyperresponsiveness were assessed on day 56. (*I*) Absolute cell numbers of eosinophils (Eos.), neutrophils (Neut.), lymphocytes (Lymph.), and macrophages (Mac.) in the BAL fluid are shown. (*J*) Airway hyperresponsiveness was assessed by measuring methacholine-induced changes in lung resistance. Mean values from four (*B*, *C*, and *E*–*G*) or five (*I* and *J*) mice per group are shown with SD or SEM. Two independent experiments were performed with similar results (*A*–*J*) (**$P < 0.01$; and *$P < 0.05$).

throughout the lung under the normal conditions (25). The majority of GFP$^+$ IL-7–producing cells within iBALT were VCAM1$^-$ and PECAM1$^+$ endothelial cells (Fig. S5*A*). Moreover, iBALT induction resulted in increased numbers of IL-7–producing cells and expression levels of *Il7* (Fig. S5 *B* and *C*). We examined differences between PECAM1$^+$GFP$^+$ and PECAM1$^+$GFP$^-$ cells by DNA microarray analysis. Isolated PECAM1$^+$GFP$^+$ (IL-7$^+$) cells showed high expression of *Pdpn*, *Prox1*, *Nrp2*, *Flt4*, and *Angptl4*, which are specific markers for LECs (Fig. 5*A*) (26). Interestingly, *Il33*, which is crucial for the pathogenesis of mucosal inflammation (27), and *Ccl19* and *Ccl21a*, key chemokines for iBALT formation (11), were also highly expressed in PECAM1$^+$GFP$^+$ cells (Fig. 5*A*). Lymphatic vessel endothelial hyaluronan receptor 1 (Lyve-1) and Podoplanin were highly expressed on the surface of PECAM1$^+$GFP$^+$ cells (Fig. 5*B*). Consistent with these findings, histological analysis revealed that IL-7–positive cells in the iBALT were located with dilated vessels that stained positive for Lyve-1 (Fig. 5*C*) (26). Moreover, we found that the majority of PECAM1$^+$Podoplanin$^+$ cells (i.e., LECs) express IL-7, but almost no expression of IL-7 was observed in PECAM1$^-$Podoplanin$^+$ cells (i.e., fibroblastic reticular cells or alveolar type I epithelial cells; Fig. 5*D* and Fig. S5*D*). These data identify an IL-7–producing LEC subset that expresses the inflammatory cytokine IL-33 and T-cell–attracting chemokines CCL19 and CCL21 within iBALT.

Next, we endeavored to find a unique cell surface marker to identify the IL-7–producing LECs in iBALT. By using a Lyoplate Screening Panel, a screening system for profiling of hundreds of murine cell surface markers by flow cytometry, we identified Thy1 (CD90) as a specific cell surface marker for the IL-7–producing cells among the PECAM1$^+$ cell population. High expression of Thy1 on the PECAM1$^+$GFP$^+$ IL-7–producing cells but not PECAM1$^+$GFP$^-$ IL-7–nonproducing cells was identified (Fig. 5*E*). Thy1-positive endothelial cells from the lung expressed significantly higher levels of IL-7 than Thy1-negative endothelial cells or VCAM1-positive stromal cells in the lung (Fig. 5*F*). Consistent with the previous reports that showed Thy1 is expressed on LECs in the lung (28, 29), our data indicate that Thy1 can be used as a useful marker for IL-7–producing LECs in the lung.

IL-7 Produced from LECs Is Required for the Maintenance of Memory Th2 Cells in the Lung. To investigate the role of IL-7 produced from LECs, we generated *Il-7flox/flox* mice crossed with *Tie2*-Cre Tg mice (*Tie2-Cre*$^+$*Il-7*$^{fl/fl}$ mice), which lack *Il-7* expression in blood endothelial cells (BECs) and LECs. The expression level of *Il-7* is very low in BECs (25), and therefore *Tie2-Cre*$^+$*Il-7*$^{fl/fl}$

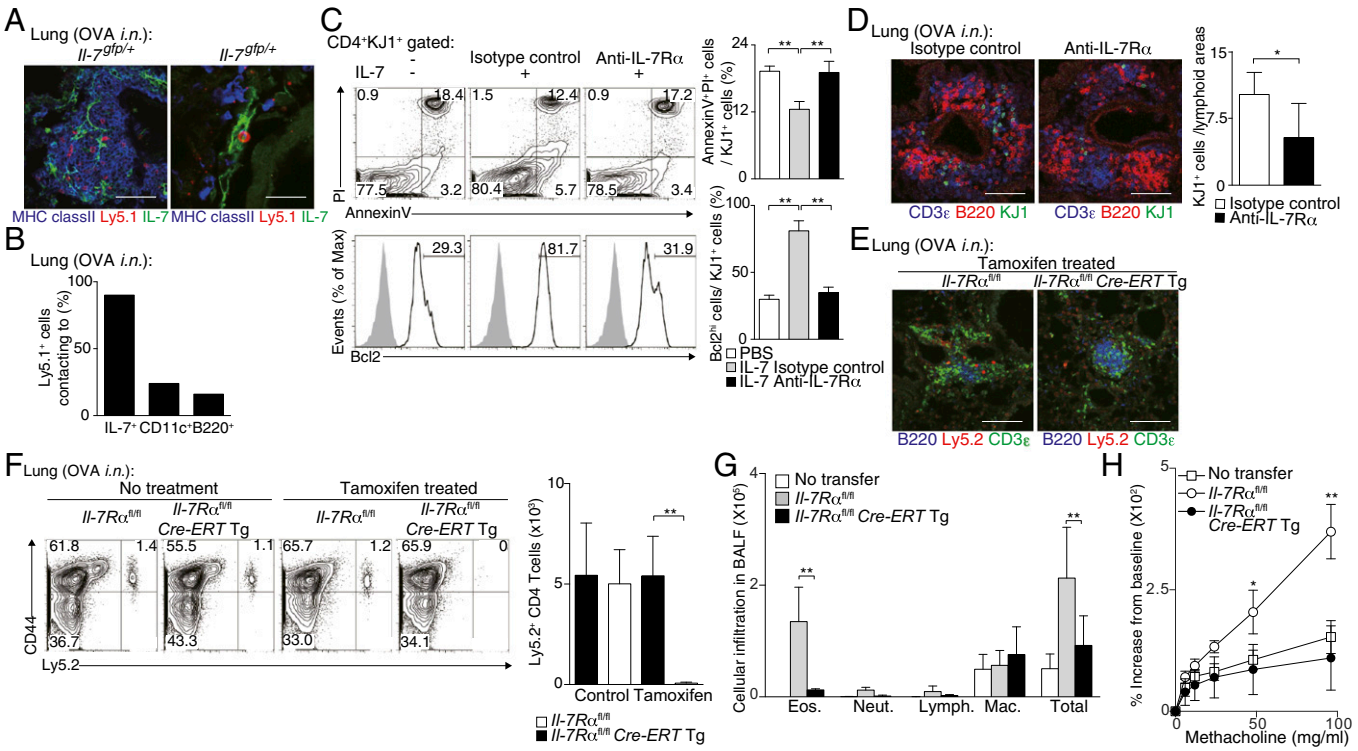

Fig. 4. IL-7 controls persistence of iBALT-residing memory Th2 cells. (*A*) Effector Th2 cells from Ly5.1 × OT-II Tg mice were transferred into IL-7:GFP knock-in mice (*Il-7*$^{gfp/+}$). Mice were challenged i.n. with OVA on days 1 and 3 and assessed on day 42. Representative confocal micrograph of lung tissue stained with anti-GFP:IL-7 (green), anti-MHC class II (blue), and anti-Ly5.1 (red) are shown. (Scale bars: *Left*, 100 μm; *Right*, 20 μm.) (*B*) Quantification analysis of memory Th2 cells (Ly5.1$^+$) proximal to IL-7$^+$, CD11c$^+$, or B220$^+$ cells in the host lung is shown. (*C*) Representative FACS plots of Annexin V and PI staining (*Upper*) and Bcl2 expression (open histogram) (*Lower*) by KJ1$^+$CD4$^+$ cells are shown. Percentages of Annexin V$^+$PI$^+$ cells (*Upper Right*) and Bcl2^{hi} cells (*Lower Right*) in the KJ1$^+$CD4$^+$ population are shown. (*D*) IL-7Rα–specific antibody or isotype control antibody was administered i.n. every second day, starting from day 42 after Th2 cell transfer, and mice were assessed at day 49. Representative confocal micrograph of iBALT in the lung tissue from mice treated with anti–IL-7Rα antibody and stained with anti-B220 (red), anti-CD3ε (blue), and anti-KJ1 (green) are shown (*Left*). Quantification analysis of KJ1$^+$ cells localized in lymphoid areas of the lungs is shown (*Right*). (Scale bars, 100 μm.) (*E–H*) Effector Th2 cells from Ly5.2 *Il-7Rα*$^{fl/fl}$ × OT-II Tg (*Il-7Rα*$^{fl/fl}$) mice or Ly5.2 *Il-7Rα*$^{fl/fl}$ × *Cre-ERT* Tg × OT-II Tg (*Il-7Rα*$^{fl/fl}$*Cre-ERT*Tg) mice were transferred into Ly5.1 mice. Mice were challenged i.n. with OVA on days 1 and 3 and assessed on day 42. Tamoxifen was injected i.p. on days 42–46 and 49–53, and mice were analyzed on day 56 (*E* and *F*) or challenged i.n. with OVA on days 56 and 58, and BAL fluid and airway hyperresponsiveness were assessed on day 59 (*G* and *H*). (*E*) Representative confocal micrographs of lung tissue stained with anti-B220 (blue), anti-CD3ε (green), and anti-Ly5.2 (red) are shown. (Scale bars, 100 μm.) (*F*) Representative staining profiles of Ly5.2 and CD44 expression on CD4$^+$ cells are shown (*Left*) with absolute cell numbers of memory Th2 cells (Ly5.2$^+$) in the lungs (*Right*). (*G*) Absolute cell numbers of eosinophils (Eos.), neutrophils (Neut.), lymphocytes (Lymph.), and macrophages (Mac.) in the BAL fluid are shown. (*H*) Airway hyperresponsiveness was assessed by measuring methacholine-induced changes in lung resistance. The mean values from five (*A*, *B*, *E*, and *F*), four (*G* and *H*), or three (*D*) mice per group or technical triplicates (*C*) are shown with SD or SEM. More than two independent experiments were performed with similar results (*A–F*; $^{**}P < 0.01$; and $^{*}P < 0.05$).

mice show selective deficiency of *Il-7* in LECs. As IL-7 KO mice have defects in lymph node development (30), we assessed whether *Tie2-Cre*$^+$*Il-7*$^{fl/fl}$ mice have normal development of lymph nodes and immune cells. We confirmed the presence of lymph nodes and equivalent proportions of CD4 and CD8 T cells in the spleen, thymus, and bone marrow, and slightly altered proportions of CD4 and CD8 T cells in the inguinal lymph nodes (Fig. S6*A*) in *Tie2-Cre*$^+$*Il-7*$^{fl/fl}$ mice compared with controls. There were no differences in the numbers of B cells or DCs between *Tie2-Cre*$^+$*Il-7*$^{fl/fl}$ mice and control mice (Fig. S6 *B* and *C*). When iBALT was induced by using *Tie2-Cre*$^+$*Il-7*$^{fl/fl}$ mice as hosts (Fig. 6*A*), the numbers of antigen-specific memory Th2 cells in the lung were significantly decreased in the *Tie2-Cre*$^+$*Il-7*$^{fl/fl}$ mice group compared with the control (*Il-7*$^{fl/fl}$ mice) group ($P = 0.0286$, two-tailed Student's *t* test; Fig. 6*B*). No significant decrease in the spleen and inguinal lymph nodes was detected (Fig. 6*B* and Fig. S6*D*). An impaired iBALT formation in the lung in *Tie2-Cre*$^+$*Il-7*$^{fl/fl}$ mice was also observed (Fig. 6*C*). These results indicate that IL-7–producing LECs are important for the formation of iBALT and the maintenance of memory Th2 cells within the iBALT structures.

Ectopic Lymphoid Structures Consisting of CD45RO$^+$CD4$^+$ T Cells and IL-7$^+$IL-33$^+$ LECs Were Generated in Nasal Polyps of Patients with ECRS. To address the pathophysiological role of IL-7–producing LECs in the ectopic lymphoid structures during chronic inflammatory diseases in humans, we analyzed local inflammatory tissues from surgically resected polyps of patients with ECRS. As a control, we included the nasal mucosa in which no chronic inflammation was detected. Very little T-cell infiltration and few lymphoid structures were detected in the nasal mucosa without chronic inflammation (Fig. 7*A*, *Left*). In contrast, massive infiltration of CD3$^+$ T cells and significantly higher numbers of ectopic lymphoid structures ($P = 0.0397$, two-tailed Student's *t* test) were detected in the nasal polyps of patients with ECRS (Fig. 7*A*, *Middle* and *Right*). These ectopic lymphoid structures included a small number of B220$^+$ cells (Fig. 7*B*, *Left*, *Upper*), and the majority of accumulated CD3$^+$ T cells expressed CD4 together with CD45RO and CD69 (Fig. 7*B*, *Right*, *Upper*). Moreover, these ectopic lymphoid structures contained PECAM1$^+$ cells and HLA-DR$^+$ cells in the areas coincident with T-cell accumulation (Fig. 7*B*, *Lower*). Importantly, Podoplanin-positive lymphatics were increased ($P < 0.0296$, two-tailed Student's *t* test) in the nasal polyps of patients with ECRS compared with the control

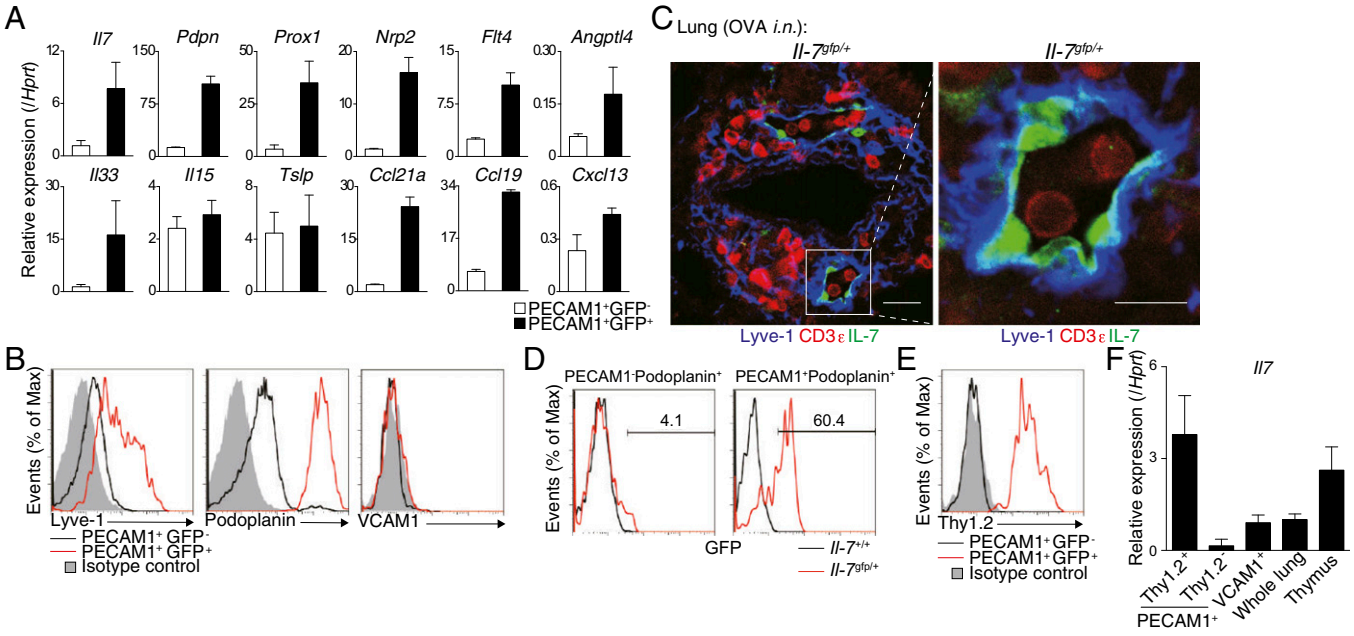

Fig. 5. Identification and characterization of IL-7–producing LECs localized in iBALT. (*A*–*D*) Effector Th2 cells from Ly5.1 OT-II Tg mice were transferred into IL-7:GFP knock-in mice (*Il-7*$^{gfp/+}$). Mice were challenged i.n. with OVA on days 1 and 3. The indicated assays were performed at day 42. (*A*) GFP$^+$ cells or GFP$^-$ cells among PECAM1$^+$ cells (a mix of lymphatic and BECs) were sorted from the lung of mice. Quantitative RT-PCR analysis of expression of the indicated genes was performed. (*B*) Representative cell surface staining profiles of PECAM1$^+$GFP$^-$ (black lines) and PECAM1$^+$GFP$^+$ cells (red lines) are shown; gray-shaded curves show staining with isotype-matched control antibody. (C) Representative confocal micrograph of lung tissue from *Il-7*$^{gfp/+}$ mice stained with anti-GFP: IL-7 (green), anti-CD3ε (red), and anti–Lyve-1 (blue). Lyve-1 expression within iBALT can be observed on the vessel-like structures and reticular cells. (Scale bars: *Left*, 20 μm; *Right*, 10 μm.) (*D*) Representative GFP expression profiles of PECAM1$^-$Podoplanin$^+$ cells and PECAM1$^+$Podoplanin$^+$ cells from the lung of *Il-7*$^{+/+}$ (black line) or *Il-7*$^{gfp/+}$ (red line) mice, gated by the strategy as described in Fig. S5*D*. (*E*) Representative cell surface staining profiles of Thy1.2 expression on PECAM1$^+$GFP$^-$ cells (black line) and PECAM1$^+$GFP$^+$ cells (red line). (*F*) PECAM1$^+$Thy1.2$^+$ cells, PECAM1$^+$Thy1.2$^-$ cells, and VCAM1$^+$ cells were sorted from the lungs of C57BL/6 mice in which iBALT had been induced as described in Fig. 1. Quantitative RT-PCR analysis of *Il7* was performed. Three technical replicates were performed for quantitative RT-PCR (*A* and *F*). More than three independent experiments were performed with similar results (*A*–*F*).

nasal mucosa (Fig. 7*C*). CD45$^-$PECAM1$^+$ cells in the nasal polyps of patients with ECRS expressed high levels of Thy1 (Fig. 7*D*). Quantitative RT-PCR revealed higher expressions of *IL7* and *IL33* in the CD45$^-$PECAM1$^+$Thy1$^+$ cells compared with CD45$^-$PECAM1$^+$Thy1$^-$ cells (Fig. 7*E*). Moreover, Podoplanin-positive lymphatics expressed Thy1 (Fig. 7*F*). These results indicate that ectopic lymphoid structures are generated in regions of chronic inflammation in human tissue such as the polyps of patients with ECRS, and increased numbers of IL-7– and IL-33–producing LECs are present within these ectopic lymphoid structures.

Discussion

Here we identify the function of iBALT as an essential structure for the accumulation and maintenance of memory Th2 cells that induce chronic allergic airway inflammation. We identified a population of Thy1$^+$IL-7–producing LECs that express the inflammatory cytokine IL-33 and T-cell–attracting chemokines CCL21 and CCL19. The Thy1$^+$IL-7–producing LECs within iBALT were found to be in direct contact with pathogenic memory Th2 cells at sites of local inflammation in the lung. Analysis of nasal polyps of patients with ECRS revealed the generation of ectopic lymphoid structures accompanied by the accumulation of IL-7– and IL-33–producing LECs together with CD45RO$^+$ memory CD4$^+$ T cells. Thus, Thy1$^+$IL-7–producing LECs in these lymphoid like structures provide a niche for memory type Tpath2 cells that induce airway inflammation.

Development of ectopic lymphoid tissues involves clustering of stromal cells that initiate formation of lymphoid structures by attracting T and B cells organized into T-cell zones and B-cell follicles with specialized populations of DCs and HEVs (8). Pulmonary infection in mice with pathogens such as influenza virus (9), murine herpesvirus 68 (12), *Mycobacterium tuberculosis* (31), modified vaccinia virus Ankara (32), or repetitive inhalations of heat-killed *Pseudomonas aeruginosa* (33) induced iBALT. These iBALTs contain myeloid DCs, a network of stromal cells, and FDCs within the B-cell follicles (12, 32, 34). The formation of HEVs and lymphatic vessels facilitates the recirculation of lymphocytes (35). In our models, we found these structures adjacent to bronchi and in close proximity to veins and arteries (Fig. 1*A*). We also detected DCs, networks of stromal cells, FDCs within B-cell follicles (Fig. 1*C*), formation of HEVs (Fig. S1*H*), and lymphatic vessels (Fig. 5*C*) within iBALT, indicating that the iBALT detected in our models is similar to that in other infection models. We have previously reported that in vitro-generated effector Th2 cells become prototypical memory Th2 cells in the spleen 4 wk after cell transfer in vivo (36). As KJ1$^+$ Th cells in the lung 42 d after cell transfer showed limited incorporation of BrdU, these cells appear to be resting memory-type Th2 cells (Fig. S1*F*). Thus, the iBALT structures characterized by the presence of Thy1$^+$IL-7–producing LECs in the lung support resting memory Th2 cells for long periods of time. Thy1$^+$IL-7–producing LECs may also play an important role in the generation of the iBALT structure itself because they express high levels of the homeostatic chemokines CCL19 and CCL21 (ligands for CCR7), which are known to recruit T cells and promote the development of lymphoid architecture (8).

In our original protocol, we used adoptive transfer of 1×10^7 effector Th2 cells, and this may result in different consequences compared with in vivo-generated Th2 responses. Reduction of the numbers of transferred OVA-specific naive CD4$^+$ T cells to 1×10^6 resulted in less memory CD4 T cells in the lung and formation of smaller iBALTs (Fig. 1 vs. Fig. S2). However, in both

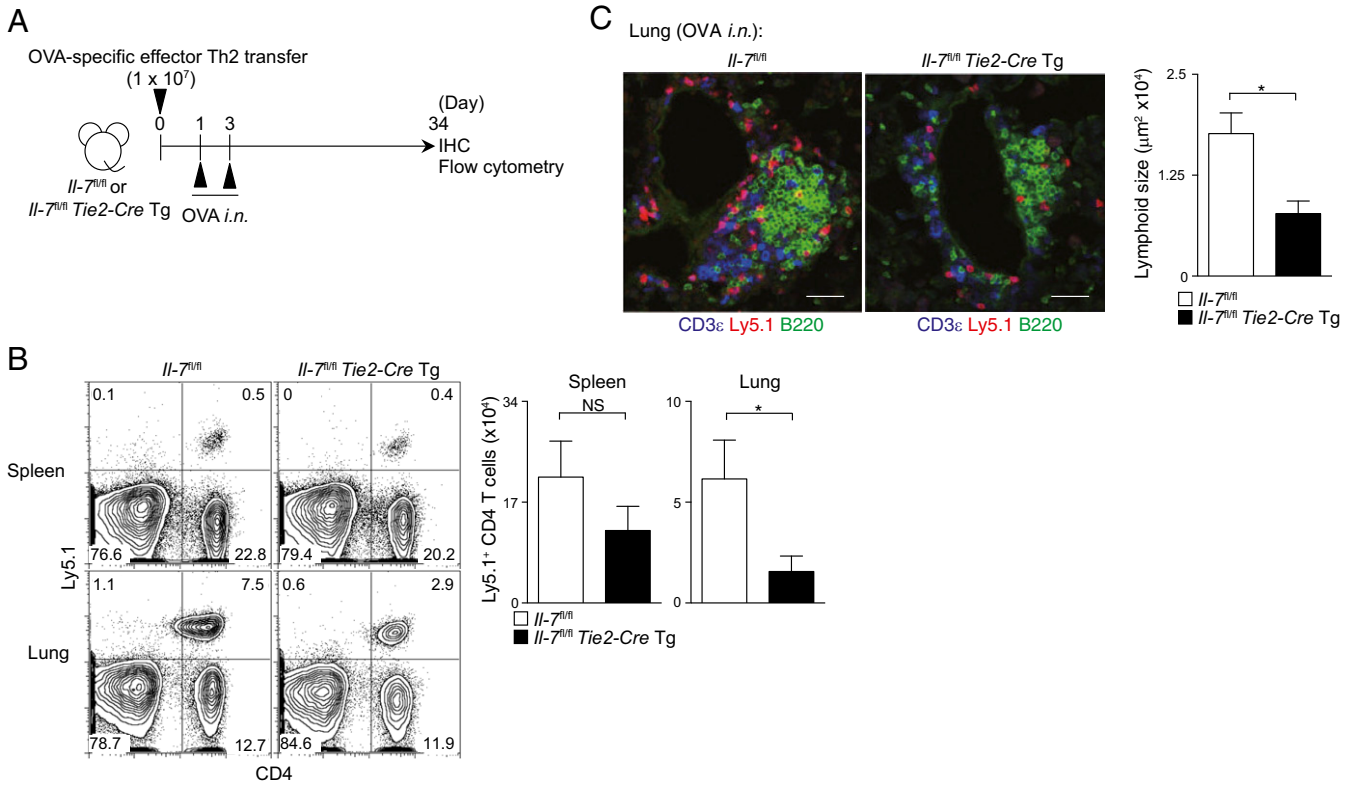

Fig. 6. LEC-derived IL-7 functions to maintain memory Th2 cells in the lung. (*A*) Effector Th2 cells from Ly5.1 OT-II Tg mice were transferred into *Il-7*$^{fl/fl}$ mice or *Il-7*$^{fl/fl}$ × *Tie2-Cre*Tg mice. Mice were challenged i.n. with OVA on days 1 and 3 and assessed on day 34. (*B*) Representative staining profiles of Ly5.1 and CD4 are shown (*Left*) with absolute cell numbers of memory Th2 cells (Ly5.1$^+$) in the lungs (*Right*). The mean values from five mice per group are shown with SD. (*C*) Representative confocal micrographs of lung tissues stained with anti-B220 (green), anti-CD3ε (blue), and anti-Ly5.1 (red) are shown (*Left*). Quantification of lymphoid areas of the lungs were assessed by immunofluorescence microscopy (*Right*) (**$P < 0.01$; and *$P < 0.05$). (Scale bars, 40 μm.) Two independent experiments were performed with similar results (*B* and *C*).

models, increased numbers of memory CD4 T cells were detected in the lung of the mice that received i.n. OVA/LPS. When we transferred equal numbers of unprimed polyclonal CD4 T cells and OVA-specific effector Th2 cells together, the unprimed polyclonal CD4 T cells did not persist as well as OVA-specific effector Th2 cells (Fig. S4*B* vs. Fig. S4*C*), indicating that effector Th2 cells may have a survival advantage in vivo compared with unprimed polyclonal CD4 T cells. However, we still found that polyclonal unprimed CD44^{hi} CD4$^+$ T cells preferentially migrated into the lung of mice with preformed iBALT (Fig. S4*C*). Thus, it is unlikely that the accumulation of memory Th2 cells in the lung after effector Th2 cell transfer is solely caused by the transfer of large numbers of Th2 cells.

IL-7 is essential for lymphocyte development and survival (37). For T cells, IL-7 is important for homeostasis and mediates the transition from effector into memory T cells (16, 23). IL-7 is produced by mesenchymal and epithelial cells such as thymic epithelial cells (38), bone marrow stromal cells (24), fibroblastic reticular cells in lymph nodes (38, 39), epidermal keratinocytes (40) and hepatocytes (41), and LECs in the lymph node (42, 43). In the present study, we identified a Thy1$^+$IL-7–producing LEC subset within the lung that supports the maintenance of memory Th2 cells in iBALT. These LECs were the major IL-7–producing cells in the iBALT, and more than 90% of memory Th2 cells were in direct contact with the IL-7–producing LECs in the lung. Consistent with previous studies showing that LECs in the lung express Thy1 (28, 29), and that IL-7 is produced by LECs (25), our data indicate that the majority of Podoplanin$^+$PECAM1$^+$ cells (i.e., LECs) are the IL-7–producing cells in the lung (Fig. 5*D*), and these cells specifically express Thy1 (Fig. 5*E*). As Thy1 is expressed on nerve fibers, fibroblasts, and T cells in the lung, the combination of PECAM1 and Thy1 staining could be a useful marker for IL-7–producing LECs. The importance of IL-7 production from LECs on the maintenance of memory Th2 cells in iBALT was confirmed by using IL-7 conditional KO mice (i.e., *Tie2*-Cre$^+$*Il-7*$^{fl/fl}$ mice). Thus, these cells likely provide a survival niche for memory Th2 cells at local inflammatory sites in the airway, similar to the IL-7–producing stromal cells in the bone marrow that was reported to be a survival niche for resting memory CD4$^+$ T cells (24, 44). As we used adoptive transfer of 1×10^7 effector Th2 cells to address the role of IL-7 for maintenance of memory Th2 cells, it is still possible that in vivo-generated smaller numbers of memory Th2 cells are less reliant on IL-7. In addition, it is reported that IL-7 exerts an important role in lymph node organogenesis and promoting lymphatic drainage (45). Less iBALT development and decreased memory T-cell accumulation detected in *Tie2*-Cre$^+$*Il-7*$^{fl/fl}$ mice could also be caused by indirect effects on lymphocyte trafficking or Th2 cell activation and maintenance in the mediastinal lymph node, or on various stromal cell structures needed for migration or retention of memory Th2 cells within iBALT. IL-7 could also indirectly regulate DC development and decrease the number of memory Th2 cells detected in *Tie2*-Cre$^+$*Il-7*$^{fl/fl}$ mice. We detected similar numbers of B220$^+$ cells, CD11c$^+$ cells, and Siglec F$^-$CD11c$^+$ cells in *Tie2*-Cre$^+$*Il-7*$^{fl/fl}$ mice compared with controls (Fig. S6 *B* and *C*), indicating that the total numbers of DCs are not changed by loss of IL-7 in LECs. However, it remains possible that DC function is altered in these mice (46). A direct effector role for locally produced IL-7 in allergic diseases has remained unclear, but elevated IL-7 was reported in the BAL fluid of subjects with allergic asthma (47).

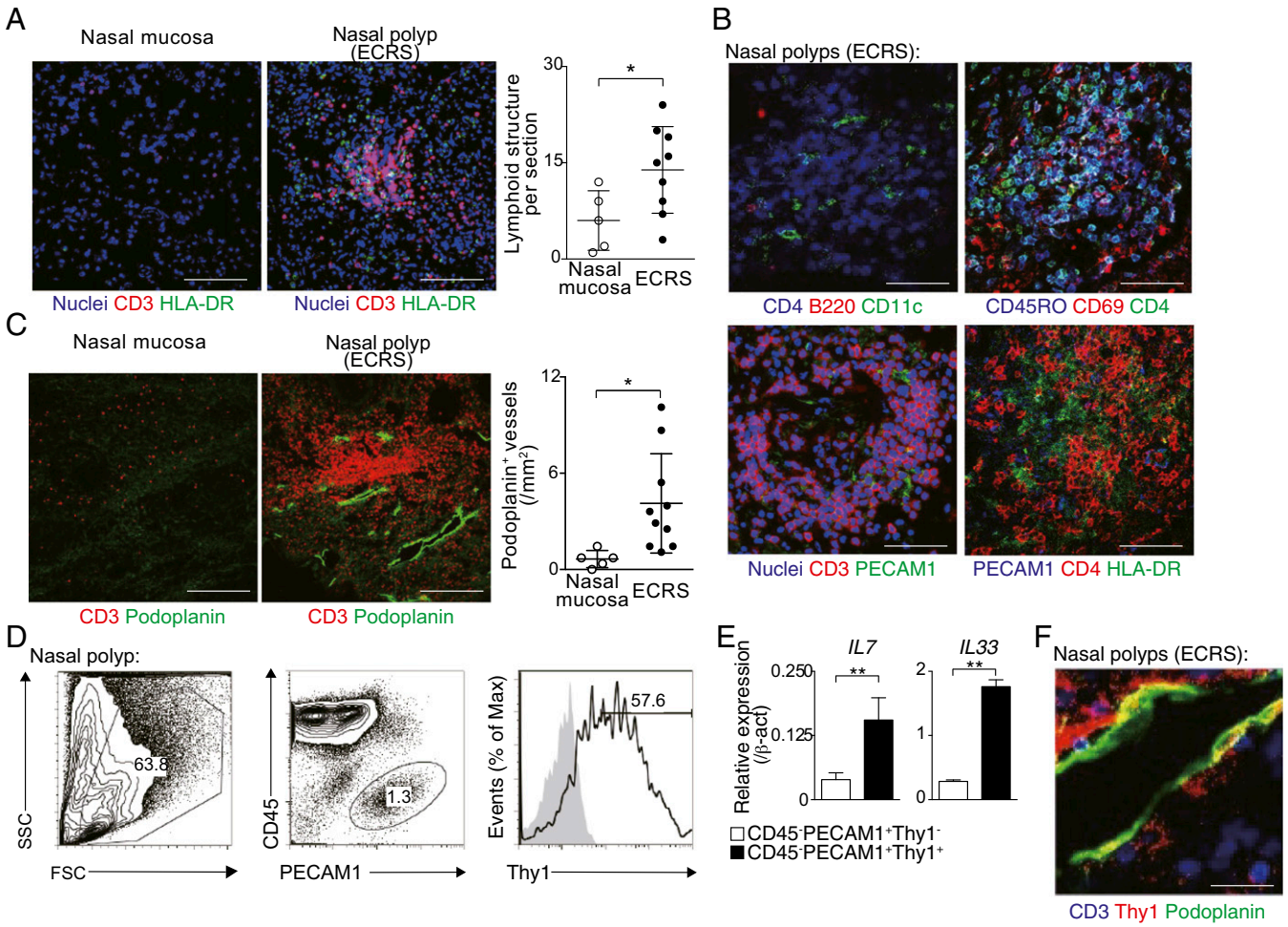

Fig. 7. Thy1$^+$IL-7–producing LECs were increased in ectopic lymphoid tissue of nasal polyps from patients with ECRS. (*A*) Representative confocal micrograph of nasal polyp tissues from patients with ECRS and normal nasal mucosa stained with anti–HLA-DR (green), anti-CD3 (red), and TO-PRO3 (blue) (*Left* and *Middle*). Quantification analysis of aggregated lymphoid structures in nasal polyp tissues is shown (*Right*) (mean ± SD; $n = 5$ for normal mucosa, $n = 9$ for ECRS). (Scale bars, 100 μm.) (*B*) Representative confocal micrograph of nasal polyp tissues from patients with ECRS stained with anti-B220 (red), anti-CD4 (blue), and anti-CD11c (green) (*Upper Left*); anti-CD69 (red), anti-CD45RO (blue), and anti-CD4 (green) (*Upper Right*); anti-PECAM1 (green), anti-CD3 (red), and TO-PRO3 (blue) (*Lower Left*); or anti-HLA-DR (green), anti-CD4 (red), and anti-PECAM1 (blue) (*Lower Right*). Two independent experiments were performed with similar results. (Scale bars, 20 μm.) (*C*) Representative confocal micrographs of the nasal polyp tissue from patients with ECRS and normal nasal mucosa stained with anti-Podoplanin (green) and anti-CD3 (red) (*Left* and *Middle*), quantification analysis of Podoplanin$^+$ lymphatics is shown (*Right*) (mean ± SD; $n = 5$ for normal mucosa, $n = 10$ for ECRS). (Scale bars, 100 μm.) (*D*) Representative staining profiles of CD45, PECAM1, and Thy1 on nasal polyp tissues from the patients with ECRS are shown. (*E*) Quantitative RT-PCR analysis of *IL7* and *IL33* expression in CD45$^-$PECAM1$^+$Thy1$^+$ cells and CD45$^-$PECAM1$^+$Thy1$^-$ cells sorted from nasal polyp tissues from the patients with ECRS are shown. Three technical replicates were performed with quantitative RT-PCR. Two independent experiments were performed with similar results (*D* and *E*). (*F*) Representative confocal micrograph of the nasal polyp tissues from patients with ECRS stained with anti-Podoplanin (green), anti-CD3 (blue), and anti-Thy1 (red). (Scale bars, 20 μm.) Two independent experiments were performed with similar results (**$P < 0.01$; and *$P < 0.05$).

Thus, our study provides a strong rationale for further investigation of the contribution of IL-7– to T-cell–mediated lung inflammation.

Early studies indicated that antigen-induced TCR signaling results in proliferation of memory CD4$^+$ T cells and contributes to the maintenance of the memory CD4$^+$ T-cell pool (22). However, the memory Th2 cells in iBALT in our experimental system were maintained in an IL-7–dependent manner, and by an antigen-independent mechanism. Memory T cells localized in the periphery, particularly at the sites near the mucosal barrier, are likely to be exposed often to stimulants including antigens, ligands for TLR, and cytokines, including those secreted from other lymphocytes (48), and may acquire distinct characteristics from memory T cells maintained in lymphoid organs. In fact, memory Th2 cells proliferate in response to IL-2 and IL-4 produced by invariant natural killer T (iNKT) cells activated with ligands, including a bacterial glycolipid, GSL1, and alter their phenotype to induce type1 inflammation (48). In the present study, we found that memory Th2 cells within iBALT are maintained in a unique microenvironment with IL-7– and IL-33–producing LEC. IL-33 is a proinflammatory cytokine that initiates chronic inflammation in the lung (49), and the IL-33 receptor is highly expressed on memory Th2 cells (4, 50). Moreover, it has been shown that IL-33 directly instructs memory type Tpath2 cells to produce IL-5 and induces eosinophilic inflammation (50, 51). Thus, we believe that IL-33 signaling is crucial for the maintenance of functions of memory Th2 cells in iBALT in the lung.

In humans, ectopic lymphoid structures often develop at sites of inflammation caused by infection, cancer, and autoimmunity (52). However, the induction and pathological nature of ectopic lymphoid structures in chronic allergic diseases was largely unknown. ECRS is a chronic upper-respiratory airway allergic

disease characterized by high IL-5 levels together with the formation of recurrent nasal polyps (53). We found increased formation of ectopic lymphoid tissues and increased IL-7–producing LECs in the nasal polyps of patients with ECRS. Moreover, we detected memory Th ($CD45RO^+CD4^+$) cells together with $HLA\text{-}DR^+$ and $PECAM1^+$ cells in ectopic lymphoid tissues of patients with ECRS, similar to that found in iBALT in mice. Interestingly, B-cell follicles, a characteristic feature of iBALT in the mouse system, were not obviously found in the ectopic lymphoid structures of patients with ECRS. However, this may be dependent on the specific pathology of the patients, because one study has identified B-cell follicle formation in nasal polyps (54). Increased lymphatics were also observed in human and mouse iBALT. This is consistent with the previous findings that influenza virus infection-induced iBALT areas have $Lyve\text{-}1^+$ lymphatic vessels (8), and robust lymphangiogenesis occurs after iBALT formation in the lungs of mice (55). In addition, increased $M2A^+$ lymphatic vessels were observed in lung biopsies from patients with rheumatoid arthritis (13).

In summary, our study demonstrates a new paradigm for how inflammatory pathogenic memory Th2 cells (i.e., Tpath2 cells) are maintained at local sites of inflammation, particularly within ectopic lymphoid tissues in the airway. We identified $Thy1^+$IL-7–producing LECs that express IL-33, CCL19, and CCL21 that appear to play a crucial role in the maintenance of Tpath2 cells in murine and human systems. The cell components that organize and contribute to iBALT formation and the functional molecules that maintain pathogenic inflammatory memory Th2 cells are therefore likely to be excellent targets for the treatment of chronic allergic airway inflammation.

Materials and Methods

Mice. BALB/c and C57BL/6 mice were purchased from CLEA Japan. The animals used in this study were backcrossed to BALB/c or C57BL/6 mice 10 times. IL-7:GFP-reporter mice (43), *Il-7Rα*$^{fl/fl}$ mice (56), and *Il-7*$^{fl/fl}$ mice (57) were previously reported. *Il-7Rα*$^{fl/fl}$ mice were crossed with *Rosa:Cre-ERT* mice (TaconicArtemis) and OTII-TCR-αβTg mice. *Il-7Rα*$^{fl/fl}$ × OT-II Tg (control) mice and *Il-7Rα*$^{fl/fl}$*Rosa:Cre-ERT* × OT-II Tg (*Il-7Rα*cKO) mice were compared. *Il-7*$^{fl/fl}$ mice were crossed with *Tie2*-Cre Tg mice (58). *Il-7*$^{fl/fl}$ mice and *Tie2*-Cre$^+$*Il-7*$^{fl/fl}$ mice were compared. Anti-OVA–specific TCR-αβ (DO11.10) Tg mice were provided by Dennis Loh (Washington University, St. Louis, MO) (59). We also used mice expressing OTII-TCR-αβ specific for residues 323–339 of the OVA protein, and Thy1.1 mice were from Jackson Laboratories. Ly5.1 mice were purchased from Sankyo Laboratory. Animal care was conducted in accordance with the guidelines of Chiba University. All animal experiments were approved by the Chiba University Review Board for Animal Care.

Flow Cytometry and Antibodies. Single-cell suspensions were prepared from spleen and lung of individual mice. For cell staining, cells were stained for 20 min at 4 °C with monoclonal antibodies specific for CD3ε (145-2C11), CD4 (RM4-5), B220 (RA3-6B2), CD45 (30-F11), CD45.1 (A20), CD45.2 (104), VCAM1 (429), IL-7Rα (SB/199), IL-7Rα (A7R34), CD31 (390), Thy1.1 (OX-7), Thy1.2 (30-H12), CD11c (HL3), and isotype control were purchased from BD; those specific for OVA-TCR (KJ1.26), MHC class II (M5/114), Lyve-1 (ALY7), and Podoplanin (8.1.1) were purchased from eBioscience; and those specific for TER119 and CD44 (IM7) were purchased from BioLegend. To exclude dead cells, we stained with 1 μg/mL propidium iodide (PI; Sigma). Stained samples were analyzed on a FACSCantoII flow cytometer (BD). Flow cytometric data were analyzed with FlowJo software (Tree Star).

Induction of iBALT Formation. Effector Th2 cells were generated as previously described (60). In brief, splenic $CD62L^+CD44^-$ naive $KJ1^+CD4^+$ T cells from DO11.10 Tg mice were stimulated with an OVA peptide (Loh15, 0.3 μM) plus antigen-presenting cells (APC) (irradiated splenocytes) under Th2 culture conditions [IL-2 (25 U/mL), IL-4 (100 U/mL) and anti–IFN-γ mAb (BioLegend)] for 6 d in vitro. Effector Th2 cells (1×10^7) were transferred i.v. into BALB/c recipient mice on day 0. On days 1 and 3, PBS or OVA solution (100 μg) was administrated i.n. or i.p. to each mouse. More than 42 d after the cell transfer, lungs were recovered and infused with 10% (vol/vol) formalin in PBS solution for H&E staining or infused with 4% (wt/vol) paraformaldehyde (PFA) in PBS solution for immunofluorescent staining. For LPS-dependent induction of iBALT, PBS solution or LPS (10 μg; Invivogen) was administrated i.n. to BALB/c mice at days 1 and 3. At day 59, lungs were recovered for flow cytometric analysis or infused with 4% (wt/vol) PFA in PBS solution for immunofluorescent staining.

Lung Dissociation and Cell Sorting. Mice were killed by anesthesia and perfused with 5 mL cold PBS solution through the right ventricle. Lungs were transferred to a tube containing ice-cold digestion buffer [RPMI 1640 supplemented with collagenase type III (200 U/mL; Worthington) and DNase I (200 μg/mL; Sigma-Aldrich)] and kept at 4 °C until digestion. Individual lungs were dissociated in 3 mL digestion buffer using a GentleMACS tissue dissociator (Miltenyi Biotec). This was followed by incubation for 30 min at 37 °C with frequent agitation and a final GentleMACS dissociation. Lung mononuclear cells were separated by centrifugation on Percoll (GE Healthcare). For sorting of lung IL-7–producing cells, lungs from IL-7:GFP knock-in mice were dissociated with a Lung Dissociation Kit (mouse; Miltenyi Biotec) by using a GentleMACS tissue dissociator (Miltenyi Biotec) according to the manufacturer's protocol. Cell suspensions were passed through a 70-μm cell strainer (Greiner Bio-One), and cells were pelleted by centrifugation. Cells were stained with anti-CD45 (30-F11; BD), anti-TER119 (TER119; BioLegend), anti-B220 (RA3-6B2; BD), and anti-PECAM1 (390; eBioscience). $PECAM1^+GFP^+$ (IL-7–producing) cells were purified by sorting (FACSAria II; BD).

Immunofluorescent Staining and Confocal Microscopy. For immunofluorescent staining, samples were fixed in 4% (wt/vol) PFA and equilibrated in 30% sucrose/PBS solution. Cryostat sections of lungs were stained and mounted with Fluorescence Mounting Medium (DakoCytomation). All immunofluorescent histological analyses were carried out with a confocal laser microscope (LSM710; Carl Zeiss). GFP expression in IL-7:GFP-reporter mice was detected by using polyclonal antibody against GFP (Invitrogen) (61). Monoclonal antibodies against CD4 (RM4-5), anti-B220 (RA3-6B2), anti-CD21 (7G6), anti-CD3ε (145-2C11), anti-Thy1.1 (OX-7), anti-CD45.1 (A20), anti-CD45.2 (104; BD), anti-MHC class II (M5/114.15.2) and anti–OVA-TCR (KJ1.26; eBioscience) and anti-CD11c (N418; BioLegend) were used for staining. Polyclonal antibody against Lyve-1 (R&D Systems) was used. For secondary antibodies, Alexa Fluor 488, Alexa Fluor 555, or Alexa Fluor 647 anti-rabbit IgG antibodies (Invitrogen) and Alexa Fluor 647 anti-goat IgG antibodies (Invitrogen) were used. Images were analyzed by ImageJ software (National Institutes of Health).

Assessment of Nasal Polyp Tissues from Patients with ECRS. Nasal polyp tissues were obtained during endoscopic sinus surgery from the patients with ECRS as previously described (62). Briefly, freshly obtained nasal polyps were immediately minced and incubated in RPMI 1640 medium containing 1 mg/mL collagenase, 0.5 mg/mL hyaluronidase, and 0.2 mg/mL DNase I (Sigma-Aldrich). Cells were then stained with anti-CD45 (HI30), anti-CD31 (WM59), and anti-Thy1 (5E10; BD) before cell sorting. For histological analysis, nasal polyp tissues were fixed in 4% paraformaldehyde and equilibrated in 30% sucrose/PBS solution. Cryostat sections of nasal polyp tissues were stained and mounted with Fluorescence Mounting Medium (DakoCytomation). Monoclonal antibodies used for immunofluorescent staining were anti-CD3 (UCHT1), anti-CD45RO (UCHL1), anti-CD69 (FN50), anti-CD4 (RPA-T4), or anti–HLA-DR (G46-6) from BD, anti-Thy1 (F15-42–1; AbD Serotec), and anti-Podoplanin (NC-08, BioLegend), and polyclonal antibody used was anti-PECAM1 (Santa Cruz). For secondary antibodies, Alexa Fluor 647 anti-rabbit IgG antibodies (Invitrogen) and Alexa Fluor 488 or Alexa Fluor 647 anti-goat IgG antibodies (Invitrogen) were used. TO-PRO3 (Invitrogen) was used to stain cell nuclei. All patients signed informed consent forms, and the study was approved by Ethics Committee of the Chiba University Graduate School of Medicine and each participating hospital.

Statistical Analyses. We expressed data as mean ± SD or mean ± SEM. Statistical analysis was performed with GraphPad Prism. Differences were determined by using the two-tailed Student *t* test, Tukey's multiple comparisons test, or two-way ANOVA with Tukey's multiple comparison test. A P value <0.05 was considered statistically significant.

Further details regarding study materials and methods are provided in *SI Materials and Methods*.

ACKNOWLEDGMENTS. We thank Hiroshi Kiyono (University of Tokyo), Shintaro Sato (University of Tokyo), and Magdalene Papadopoulos for critical review of the manuscript; Yuri Nakamura and Toshihiro Ito for their excellent technical assistance; and Yoko Ozawa for animal husbandry. This work was supported by the Global COE (Center of Excellence) Program (Global Center for Education and Research in Immune System Regulation and Treatment); Ministry of Education, Culture, Sports, Science and Technology (MEXT Japan) Grants-in-Aid for Scientific Research (S) 26221305, (B) 21390147,

(C) 24592083; Young Scientists (B) 24790461 and 25860352; and Research Activity start-up 23890030 and 25893032; the Ministry of Health, Labor and Welfare; the Practical Research Project for Allergic Diseases and Immunology (Research on Allergic Diseases and Immunology) from the Japan Agency for Medical Research and Development; AMED; The Astellas Foundation for Research on Metabolic Disorders; The Uehara Memorial Foundation; Osaka Foundation for Promotion of Fundamental Medical Research; Kanae Foundation for the Promotion of Medical Science; Princess Takamatsu Cancer Research Fund; Takeda Science Foundation; The Naito Foundation; and Japanese Society for the Promotion of Science Postdoctoral Fellowship 2109747 (to D.J.T.).

1. Crotty S, Kersh EN, Cannons J, Schwartzberg PL, Ahmed R (2003) SAP is required for generating long-term humoral immunity. *Nature* 421(6920):282–287.
2. Francus T, Francus Y, Siskind GW (1991) Memory T cells enhance the expression of high-avidity naive B cells. *Cell Immunol* 134(2):520–527.
3. Sun JC, Williams MA, Bevan MJ (2004) CD4+ T cells are required for the maintenance, not programming, of memory CD8+ T cells after acute infection. *Nat Immunol* 5(9): 927–933.
4. Endo Y, et al. (2011) Eomesodermin controls interleukin-5 production in memory T helper 2 cells through inhibition of activity of the transcription factor GATA3. *Immunity* 35(5):733–745.
5. Islam SA, et al. (2011) Mouse CCL8, a CCR8 agonist, promotes atopic dermatitis by recruiting IL-5+ T(H)2 cells. *Nat Immunol* 12(2):167–177.
6. Endo Y, Hirahara K, Yagi R, Tumes DJ, Nakayama T (2014) Pathogenic memory type Th2 cells in allergic inflammation. *Trends Immunol* 35(2):69–78.
7. Sminia T, van der Brugge-Gamelkoorn GJ, Jeurissen SH (1989) Structure and function of bronchus-associated lymphoid tissue (BALT). *Crit Rev Immunol* 9(2):119–150.
8. Carragher DM, Rangel-Moreno J, Randall TD (2008) Ectopic lymphoid tissues and local immunity. *Semin Immunol* 20(1):26–42.
9. Moyron-Quiroz JE, et al. (2004) Role of inducible bronchus associated lymphoid tissue (iBALT) in respiratory immunity. *Nat Med* 10(9):927–934.
10. GeurtsvanKessel CH, et al. (2009) Dendritic cells are crucial for maintenance of tertiary lymphoid structures in the lung of influenza virus-infected mice. *J Exp Med* 206(11): 2339–2349.
11. Rangel-Moreno J, Moyron-Quiroz JE, Hartson L, Kusser K, Randall TD (2007) Pulmonary expression of CXC chemokine ligand 13, CC chemokine ligand 19, and CC chemokine ligand 21 is essential for local immunity to influenza. *Proc Natl Acad Sci USA* 104(25):10577–10582.
12. Kocks JR, Davalos-Misslitz AC, Hintzen G, Ohl L, Förster R (2007) Regulatory T cells interfere with the development of bronchus-associated lymphoid tissue. *J Exp Med* 204(4):723–734.
13. Rangel-Moreno J, et al. (2006) Inducible bronchus-associated lymphoid tissue (iBALT) in patients with pulmonary complications of rheumatoid arthritis. *J Clin Invest* 116(12):3183–3194.
14. Hogg JC, et al. (2004) The nature of small-airway obstruction in chronic obstructive pulmonary disease. *N Engl J Med* 350(26):2645–2653.
15. Ulrichs T, et al. (2004) Human tuberculous granulomas induce peripheral lymphoid follicle-like structures to orchestrate local host defence in the lung. *J Pathol* 204(2): 217–228.
16. Benninger MS, et al. (2003) Adult chronic rhinosinusitis: Definitions, diagnosis, epidemiology, and pathophysiology. *Otolaryngol Head Neck Surg* 129(3, suppl):S1–S32.
17. Bachert C, et al. (2004) Allergic rhinitis, rhinosinusitis, and asthma: One airway disease. *Immunol Allergy Clin North Am* 24(1):19–43.
18. Meltzer EO, et al.; Rhinosinusitis Initiative (2006) Rhinosinusitis: Developing guidance for clinical trials. *J Allergy Clin Immunol* 118(5, suppl):S17–S61.
19. Hamilos DL (2011) Chronic rhinosinusitis: Epidemiology and medical management. *J Allergy Clin Immunol* 128(4):693–707; quiz 708-699.
20. Hamilos DL, et al. (2001) GRbeta expression in nasal polyp inflammatory cells and its relationship to the anti-inflammatory effects of intranasal fluticasone. *J Allergy Clin Immunol* 108(1):59–68.
21. Woodland DL, Kohlmeier JE (2009) Migration, maintenance and recall of memory T cells in peripheral tissues. *Nat Rev Immunol* 9(3):153–161.
22. Seddon B, Tomlinson P, Zamoyska R (2003) Interleukin 7 and T cell receptor signals regulate homeostasis of CD4 memory cells. *Nat Immunol* 4(7):680–686.
23. Kondrack RM, et al. (2003) Interleukin 7 regulates the survival and generation of memory CD4 cells. *J Exp Med* 198(12):1797–1806.
24. Tokoyoda K, et al. (2009) Professional memory CD4+ T lymphocytes preferentially reside and rest in the bone marrow. *Immunity* 30(5):721–730.
25. Miller CN, et al. (2013) IL-7 production in murine lymphatic endothelial cells and induction in the setting of peripheral lymphopenia. *Int Immunol* 25(8):471–483.
26. Oliver G (2004) Lymphatic vasculature development. *Nat Rev Immunol* 4(1):35–45.
27. Garlanda C, Dinarello CA, Mantovani A (2013) The interleukin-1 family: Back to the future. *Immunity* 39(6):1003–1018.
28. Kretschmer S, et al. (2013) Visualization of intrapulmonary lymph vessels in healthy and inflamed murine lung using CD90/Thy-1 as a marker. *PLoS One* 8(2):e55201.
29. Jurisic G, Iolyeva M, Proulx ST, Halin C, Detmar M (2010) Thymus cell antigen 1 (Thy1, CD90) is expressed by lymphatic vessels and mediates cell adhesion to lymphatic endothelium. *Exp Cell Res* 316(17):2982–2992.
30. von Freeden-Jeffry U, et al. (1995) Lymphopenia in interleukin (IL)-7 gene-deleted mice identifies IL-7 as a nonredundant cytokine. *J Exp Med* 181(4):1519–1526.
31. Kahnert A, et al. (2007) Mycobacterium tuberculosis triggers formation of lymphoid structure in murine lungs. *J Infect Dis* 195(1):46–54.
32. Halle S, et al. (2009) Induced bronchus-associated lymphoid tissue serves as a general priming site for T cells and is maintained by dendritic cells. *J Exp Med* 206(12): 2593–2601.
33. Toyoshima M, Chida K, Sato A (2000) Antigen uptake and subsequent cell kinetics in bronchus-associated lymphoid tissue. *Respirology* 5(2):141–145.
34. Randall TD (2010) Bronchus-associated lymphoid tissue (BALT) structure and function. *Adv Immunol* 107:187–241.
35. Xu B, et al. (2003) Lymphocyte homing to bronchus-associated lymphoid tissue (BALT) is mediated by L-selectin/PNAd, alpha4beta1 integrin/VCAM-1, and LFA-1 adhesion pathways. *J Exp Med* 197(10):1255–1267.
36. Nakayama T, Yamashita M (2009) Critical role of the Polycomb and Trithorax complexes in the maintenance of CD4 T cell memory. *Semin Immunol* 21(2):78–83.
37. Ma A, Koka R, Burkett P (2006) Diverse functions of IL-2, IL-15, and IL-7 in lymphoid homeostasis. *Annu Rev Immunol* 24:657–679.
38. Zamisch M, et al. (2005) Ontogeny and regulation of IL-7-expressing thymic epithelial cells. *J Immunol* 174(1):60–67.
39. Link A, et al. (2007) Fibroblastic reticular cells in lymph nodes regulate the homeostasis of naive T cells. *Nat Immunol* 8(11):1255–1265.
40. Matsue H, Bergstresser PR, Takashima A (1993) Keratinocyte-derived IL-7 serves as a growth factor for dendritic epidermal T cells in mice. *J Immunol* 151(11):6012–6019.
41. Sawa Y, et al. (2009) Hepatic interleukin-7 expression regulates T cell responses. *Immunity* 30(3):447–457.
42. Malhotra D, et al.; Immunological Genome Project Consortium (2012) Transcriptional profiling of stroma from inflamed and resting lymph nodes defines immunological hallmarks. *Nat Immunol* 13(5):499–510.
43. Hara T, et al. (2012) Identification of IL-7-producing cells in primary and secondary lymphoid organs using IL-7-GFP knock-in mice. *J Immunol* 189(4):1577–1584.
44. Shinoda K, et al. (2012) Type II membrane protein CD69 regulates the formation of resting T-helper memory. *Proc Natl Acad Sci USA* 109(19):7409–7414.
45. Iolyeva M, et al. (2013) Interleukin-7 is produced by afferent lymphatic vessels and supports lymphatic drainage. *Blood* 122(13):2271–2281.
46. Guimond M, et al. (2009) Interleukin 7 signaling in dendritic cells regulates the homeostatic proliferation and niche size of CD4+ T cells. *Nat Immunol* 10(2):149–157.
47. Kelly EA, et al. (2009) Potential contribution of IL-7 to allergen-induced eosinophilic airway inflammation in asthma. *J Immunol* 182(3):1404–1410.
48. Iwamura C, et al. (2012) Regulation of memory CD4 T-cell pool size and function by natural killer T cells in vivo. *Proc Natl Acad Sci USA* 109(42):16992–16997.
49. Lloyd CM (2010) IL-33 family members and asthma - bridging innate and adaptive immune responses. *Curr Opin Immunol* 22(6):800–806.
50. Endo Y, et al. (2015) The interleukin-33-p38 kinase axis confers memory T helper 2 cell pathogenicity in the airway. *Immunity* 42(2):294–308.
51. Endo Y, Nakayama T (2015) Pathogenic Th2 (Tpath2) cells in airway inflammation. *Oncotarget* 6(32):32303–32304.
52. Pitzalis C, Jones GW, Bombardieri M, Jones SA (2014) Ectopic lymphoid-like structures in infection, cancer and autoimmunity. *Nat Rev Immunol* 14(7):447–462.
53. Gevaert P, et al. (2006) Nasal IL-5 levels determine the response to anti-IL-5 treatment in patients with nasal polyps. *J Allergy Clin Immunol* 118(5):1133–1141.
54. Hulse KE, et al. (2013) Chronic rhinosinusitis with nasal polyps is characterized by B-cell inflammation and EBV-induced protein 2 expression. *J Allergy Clin Immunol* 131(4):1075–1083.
55. Baluk P, et al. (2014) Preferential lymphatic growth in bronchus-associated lymphoid tissue in sustained lung inflammation. *Am J Pathol* 184(5):1577–1592.
56. Tani-ichi S, et al. (2013) Interleukin-7 receptor controls development and maturation of late stages of thymocyte subpopulations. *Proc Natl Acad Sci USA* 110(2):612–617.
57. Liang B, et al. (2012) Role of hepatocyte-derived IL-7 in maintenance of intrahepatic NKT cells and T cells and development of B cells in fetal liver. *J Immunol* 189(9): 4444–4450.
58. Kisanuki YY, et al. (2001) Tie2-Cre transgenic mice: A new model for endothelial cell-lineage analysis in vivo. *Dev Biol* 230(2):230–242.
59. Murphy KM, Heimberger AB, Loh DY (1990) Induction by antigen of intrathymic apoptosis of CD4+CD8+TCRlo thymocytes in vivo. *Science* 250(4988):1720–1723.
60. Kuwahara M, et al. (2012) The transcription factor Sox4 is a downstream target of signaling by the cytokine TGF-β and suppresses T(H)2 differentiation. *Nat Immunol* 13(8):778–786.
61. Hanazawa A, et al. (2013) CD49b-dependent establishment of T helper cell memory. *Immunol Cell Biol* 91(8):524–531.
62. Yamamoto H, et al. (2007) Detection of natural killer T cells in the sinus mucosa from asthmatics with chronic sinusitis. *Allergy* 62(12):1451–1455.